

Self-Sensing Self-Diagnostic Structures for Next Generation Intelligent Aerospace Systems

Fotis Kopsaftopoulos
Assistant Professor
Mechanical, Aerospace, and
Nuclear Engineering,
Rensselaer Polytechnic
Institute
Troy, NY, USA

Fu-Kuo Chang
Professor
Department of Aeronautics &
Astronautics, Stanford
University
Stanford, CA, USA

ABSTRACT

The objective of this work is to outline a novel unified design, sensing, fabrication, and data-driven modeling and analysis approach for future self-sensing self-diagnostic intelligent aerospace structures with state sensing and awareness capabilities. The experimental assessment of is resented for an intelligent composite UAV wing with embedded distributed micro-sensor networks. The sensor networks consist of piezoelectric, strain, and temperature sensors in order to enable the data-driven modeling and interpretation and structural health monitoring of the wing under varying flight states and uncertainty. Piezoelectric sensors are employed in two modes: (i) passive mode to sense the ambient vibration of the wing in order to model and interpret the structural dynamic response and relate it to critical aerodynamic/aeroelastic phenomena such as stall and flutter; (ii) active mode, as both actuators and sensors to implement an active sensing acousto-ultrasound pitch-catch SHM approach. A novel modeling approach based on the recently introduced Vector-dependent Functionally Pooled (VFP) model structure is employed for the stochastic data-driven global modeling of the wing dynamics based on a series of wind tunnel experiments. In addition, the strain distribution is established under the considered flight states and critical areas of the flight envelope are identified. The obtained results demonstrate the successful integration of the micro-fabricated stretchable sensor networks with the composite materials of the wing, as well as the effectiveness of the stochastic “global” modeling and active sensing SHM approaches, proving their integration potential for the next generation of self-sensing self-diagnostic aerospace structures.

INTRODUCTION

The next generation of intelligent aerospace structures and aerial vehicles will be able to “feel,” “think,” and “react” in real time based on high-resolution state-sensing, awareness, and self-diagnostic capabilities. They will be able to sense and observe phenomena at unprecedented length and time scales allowing for improved performance, adaptability, autonomous operation, increased safety, reduced mission costs, and complete life-cycle monitoring and management. One of the main challenges of the current state-of-the-art research is the development of technologies that will lead to intelligent aerial vehicles able to (i) sense the external environment (temperature, air pressure, humidity, etc.) (Ref. 1), (ii) sense their flight and aeroelastic state (airspeed, angle of attack, aerodynamic loads, blade configuration and morphing, etc.) and internal structural condition (stresses, strains, damage) (Refs. 2–4), and (iii) effectively interpret the sensing data to achieve real-time state awareness, usage and health monitoring (Refs. 5–8).

Knowing the aerodynamic and structural loads, and health state of critical structural components, such as aircraft wings and rotorcraft blades, can be critical in the design of the next generation of self-sensing self-diagnostic structures. The integration of appropriate multifunctional composite materials with effective and robust monitoring and diagnostic approaches will enable high-resolution state sensing and awareness capabilities. Such self-sensing multifunctional materials have the potential to enable “intelligent” structural systems via the integration of HUMS and SHM systems in which a network of sensors is attached or embedded inside the composite structure. (Refs. 1, 6, 7, 9). The actual deployment of such approaches will lead to the improved performance, extended flight envelope, increased safety, and complete monitoring and life-cycle management of future aerial vehicles.

Existing usage and health monitoring approaches are based on the use of information obtained via various sensor technologies installed on critical structural and mechanical components along with corresponding diagnostic algorithms and data analytics. Using this information and corresponding processing methods, such systems can issue alerts and identify

Presented at the AHS Airworthiness and HUMS Technical Meeting, Huntsville, Alabama, USA, February 21-22, 2018.
Copyright © 2018 by AHS International, Inc. All rights reserved.

potentially dangerous states that can potentially lead to safety-critical events. The pilot or controller/flight management system may enable appropriate control actions in order to ensure system safety within the specified flight envelope that has been predetermined during the design phase. Within this context, the performance capabilities remain strictly confined within the flight envelope due to limited structural awareness, and oftentimes are rather conservative in order to ensure the safety of the system. On the other hand, the “self-sensing self-diagnostic” concept aims at the development of methods that leverage high levels of structural and aeroelastic awareness via the use of appropriate sensing, modeling and data-driven analysis techniques in order to exploit the full range of performance capabilities while ensuring the structural safety based on the “global” real-time monitoring of the vehicle.

The most critical challenge for the postulation of a complete and applicable self-diagnostic state-awareness framework for future aircraft and vertical flight systems is the effective modeling and interpretation of sensory data obtained under constantly changing dynamic environments, multiple flight states and varying structural health conditions. Evidently, all these different operating conditions have a significant impact on the structural dynamics and aeroelastic response. When it comes to the aeroelastic behavior, dynamic aeroelastic effects resulting from the interaction of the aerodynamic, elastic, and inertial forces require careful consideration throughout the design phase of the aircraft and pose a major safety-critical factor in the qualification of aircraft into service (Refs. 10–14). It is therefore evident that the flight states and operating conditions—characterized by several heterogeneous variables, such as airspeed, angle of attack (AoA), blade pitch, altitude, temperature, humidity, icing, and so on—may vary over time, and consequently affect the system dynamics and aeroelastic response. In such cases, the issue of the accurate data analysis, modeling, and interpretation under varying flight states remains a critical one that needs to be properly addressed.

In this work, the complete design, integration, and wind tunnel experimental assessment are presented for an intelligent composite high-lift low-drag wing with state-sensing and awareness capabilities. A composite UAV wing is outfitted with four stretchable sensor networks that are embedded inside the carbon/glass fiber composite layup. Each of the four sensor networks consists of 8 piezoelectric lead-zirconate titanate (PZT) sensors (disc PZTs 1/8 in diameter), 6 strain gauges, and 23 resistive temperature detectors (RTDs). The fabricated wing can sense its structural state and surrounding environment during flight and interpret the sensing information to determine its actual operating state and flight configuration. Piezoelectric sensors are used to sense the vibration of the wing and identify the coupled airflow-structural dynamics. Strain gauges are used to determine the strain distribution of the wing and identify potential critical areas for the considered experimental conditions. Wind tunnel experiments were conducted for various angles of attacks and freestream airflow velocities for the investigation of a broad regime of flight conditions and structural states. The method of approach is divided into three tasks: (i) distributed multi-modal sensor

networks for state sensing; (ii) structural design and fabrication via integrated sensor networks and composite materials; (iii) state awareness via statistical signal processing and stochastic identification techniques for data processing and interpretation; (iv) structural health monitoring via an acousto-ultrasound guided-wave-based active sensing SHM in order to detect and localize damage on the wing during its actual operation.

In this study, special emphasis is given to the data modeling and system identification via wind tunnel experiments under various flight (operating) conditions defined by multiple airspeeds and angles of attack (AoA). A novel modeling approach based on the recently introduced Vector-dependent Functionally Pooled (VFP) model structure (Refs. 7, 15, 16) is employed for the stochastic identification of the coupled airflow-structural dynamics for the complete range of the admissible flight states; that is all airspeeds and angles of attack of the wing that are considered in the wind tunnel experiments and may span the complete flight envelope. The unique characteristic of the VFP-based modeling approach is that it enables the analytical inclusion of the flight and/or structural state (see (Ref. 17)) on the coupled airflow-structural dynamics, as the model parameters depend functionally on the flight state.

DISTRIBUTED SENSOR NETWORKS AND WING INTEGRATION

Recently, micro-fabricated expandable sensor networks have been developed and deployed micro-scale sensors over macroscopic areas (Refs. 1, 9, 18–22). The component size is on the same order as an individual fiber in typical composite materials or scrim in film adhesives and small enough to be placed into a composite without structural modifications. These networks can be used in-situ, from the material fabrication throughout its service life, to monitor the cure process of composite materials, characterize material properties post-cure, and monitor the structural dynamics along with the health of the structure during its life cycle.

In this work four stretchable sensor networks with integrated distributed PZT, strain, and RTD sensors have been designed and fabricated (Refs. 1, 9, 18–21) so that they can be embedded inside the layup of the composite wing. Extensible wires connect the network nodes and serve as the signal communication channels. Before stretching, the network dimensions are 52.8 mm by 39.6 mm that after the stretching process expand to 140 mm by 105 mm yielding a 700% total surface area increase (Ref. 21). Each of the four sensor networks contains 8 piezoelectric sensors (round PZTs 3.175 mm in diameter), 6 strain gauges, and 24 RTDs. The total number of embedded sensors in the composite wing is 148.

The prototype wing was designed, constructed and tested at Stanford University. The designed wing is based on the cambered SG6043 high lift-to-drag ratio airfoil with a 0.86 m wing span, 0.235 m chord, and an aspect ratio of 7.32. In order to achieve the successful integration and fabrication of

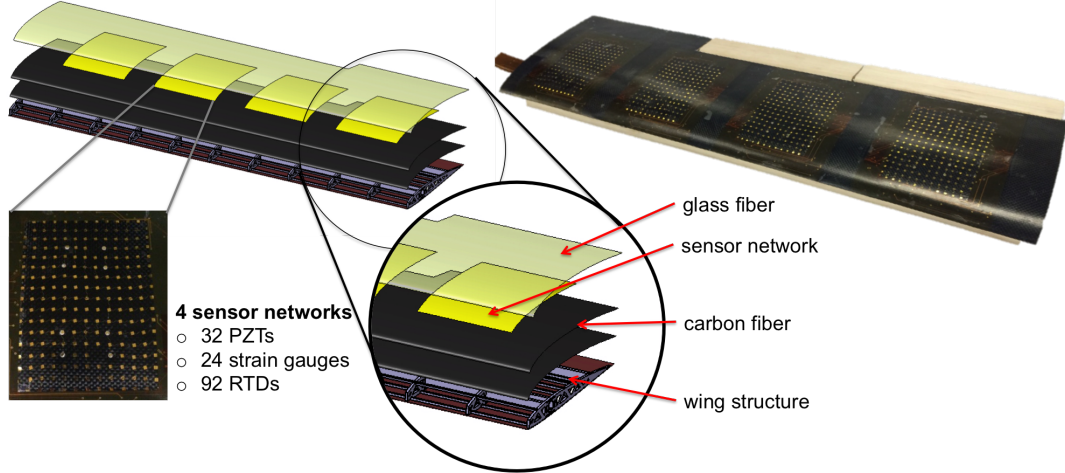


Fig. 1. The intelligent composite wing design with a total of 148 (32 piezoelectric, 24 strain gauges, and 92 RTDs) micro-sensors embedded in the composite layup.

the wing prototype, an appropriate network-material integration process had to be developed for embedding the micro-fabricated sensor networks inside the composite materials. The composite wing structure was manufactured based on carbon and glass laminated composites. The layup consists of carbon fiber (CF) plain weave fabric 1K T300 and glass fiber (GF) plain wave fabric 18 gr/m² infused with Araldite LY/HY5052 epoxy. The stacking sequence of the layers was [0° GF, 0° CF, 45° CF, 45° CF, 0° CF, 0° GF] (Figure 1). The four networks were embedded between the two top layers at 0° of the layup (near the wing surface) during the lamination process. The supporting wing structure consists of wooden (basswood) ribs and spars.

THE EXPERIMENTS

The wing was tested in the open-loop wind tunnel (WT) facility at Stanford University. The WT has a square test section of 0.84 m by 0.84 m (33 by 33 in) and can achieve continuous flow speeds up to approximately 28 m/s. A custom basis was designed and fabricated to support the wing and permit adjustments in the angle of attack (AoA). The wing was mounted horizontally inside the test section. Eight commercial strain gauges were attached on appropriate locations of the basis to measure the aerodynamic forces. The axis of rotation coincided approximately with the quarter of the wing chord. Figure 2 presents the composite wing with the corresponding locations of the PZTs and strain sensors. Table 1 presents the wing dimensions.

A series of wind tunnel experiments were conducted for various AoA and airspeeds. For each AoA, spanning the range from 0 to 18 degrees with an incremental step of 1 degree, data were sequentially collected for all velocities within the range 9 m/s to 22 m/s (incremental step of 1 m/s). The above procedure resulted to 266 different experiments covering the

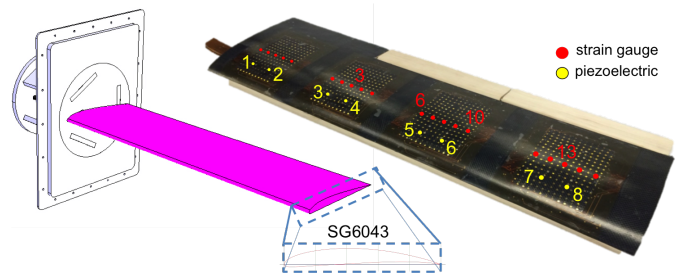


Fig. 2. The intelligent composite wing with the embedded sensor networks and the locations of the piezoelectric and strain sensors.

complete range of the considered flight states. The experimental conditions along with the Reynolds numbers are outlined in Table 2.

For each experiment the vibration and strain responses were recorded at different locations on the wing via the embedded piezoelectric sensors (initial sampling frequency $f_s = 1000$ Hz, initial signal bandwidth 0.1 – 500 Hz) and strain gauges (sampling frequency $f_s = 100$ Hz, signal bandwidth DC100 Hz), respectively. The signals were recorded via a National Instruments X Series 6366 data acquisition module featuring eight 16-bit simultaneously sampled analog-to-digital channels. The strain signals were driven through a custom designed and built signal conditioning device into the data acquisition system. The total number of the sensor signals that were obtained was limited by the available number of chan-

Table 1. Wing dimensions.

Chord c	0.235 m
Span b	0.86 m
Area S	0.2 m ²
Aspect Ratio AR	7.32

Table 2. The conditions considered in the wind tunnel experiments.

$Re (\times 10^3)$	124	155	171	187	202	217	233	248	264	280	295	311	326	342
U_∞ (m/s)	9	10	11	12	13	14	15	16	17	18	19	20	21	22

Angle of attack: 0 – 18 degrees; Total number of experiments: 266

Table 3. Data acquisition and signal pre-processing.

	Piezos	Strain gauges
Number of sensors:	8	15
Sampling frequency:	$f_s = 1000$ Hz	$f_s = 100$ Hz
Bandwidth:	[0.1 – 500] Hz	[DC – 50] Hz
Signal length:	$N = 90,000$ (90 s)	$N = 9,000$ (90 s)

nels of the data acquisition system. Table 3 presents the sensors, data acquisition, signal details.

STOCHASTIC GLOBAL MODELING

In this section the modeling of the coupled airflow-structural dynamics is addressed via the use of stochastic functionally pooled models, or more precisely Vector-dependent Functionally Pooled AutoRegressive (VFP-AR) models. These models are capable of representing the system dynamics for the complete range of flight and structural states based on data records obtained under a sample of these states. The problem is important in a number of practical applications and is tackled within a recently introduced Functional Pooling framework (Refs. 7, 15, 16, 23). This study focuses on the case of flight states characterized by two parameters, namely the airspeed and the angle of attack of the wing. For the case where the modeling of the structural state is modeled in terms of damage location and damage magnitude, the interested reader is referred to (Refs. 16, 17).

Classical system identification aims at deriving a model representing a system under a specific operating condition. Yet, in many cases, a system may operate under different conditions at different occasions (time periods), with the dynamics depending in a pseudo-static fashion on certain operating parameter(s) - also referred to as scheduling parameter(s). In such cases, given a number of data records from the system operating under a sample of different conditions, it is highly desirable to establish a single and global model, that, while compact (parsimonious), will be capable of accurately representing the dynamics under any considered condition.

Baseline Modeling under a Single Flight State

The modeling of the wing’s dynamic response under a single flight state is an initial step performed in order to facilitate (in the sense of providing approximate model orders) the subsequent step of the global modeling under all the admissible flight states. A discrete-time model (or a vector model or an array of models in the case of several vibration response measurement locations) representing the system dynamics is obtained via standard identification procedures (Refs. 24, 25).

In this study a single response AutoRegressive (AR) model is used. An $AR(n)$ model is of the form¹ (Ref. 24):

$$y[t] + \sum_{i=1}^n a_i \cdot y[t-i] = e[t] \quad e[t] \sim \text{iid } \mathcal{N}(0, \sigma_e^2) \quad (1)$$

with t designating the normalized discrete time ($t = 1, 2, 3, \dots$ with absolute time being $(t-1)T_s$, where T_s stands for the sampling period), $y[t]$ the measured vibration response signals as generated by the piezoelectric sensors of the wing, n the AR order, and $e[t]$ the stochastic model residual (one-step-ahead prediction error) sequence, that is a white (serially uncorrelated), Gaussian, zero mean with variance σ_e^2 sequence. The symbol $\mathcal{N}(\cdot, \cdot)$ designates Gaussian distribution with the indicated mean and variance, and iid stands for identically independently distributed.

The model is parameterized in terms of the parameter vector $\bar{\theta} = [a_1 \dots a_n : \sigma_e^2]^T$ to be estimated from the measured signals (Ref. 24). Model estimation may be achieved based on minimization of the Ordinary Least Squares (OLS) or the Weighted Least Squares (WLS) criteria (Ref. 24). The modeling procedure involves the successive fitting of $AR(n)$ models for increasing order n until an adequate model is selected (Ref. 26). Model order selection is based on the Bayesian Information Criterion (BIC) and the residual sum of squares normalized by the series sum of squares (RSS/SSS). Final model validation is based on formal verification of the residual (one-step-ahead prediction error) sequence uncorrelatedness (whiteness) hypothesis (Ref. 24, pp. 512-513).

Global Modeling under Multiple Flight States

The VFP-AR representation allows for complete and precise modeling of the global wing dynamics under multiple operating conditions defined by varying airspeed and angle of attack. The VFP model parameters and residual series covariance depend functionally on the airspeed and AoA, while the corresponding interrelations and statistical dependencies between the different flight states are taken into account.

The global modeling of the composite wing via a VFP-AR model involves consideration of all the admissible airspeeds and AoA that define the flight envelope of the wing. A total of $M_1 \times M_2$ experiments is performed (in this case via wind tunnel experiments; alternatively, analytical models and simulations can be used), with M_1 and M_2 designating the number of experiments under the various airspeeds and AoA, respectively. Each experiment is characterized by a specific

¹Lower case/capital bold face symbols designate vector/matrix quantities, respectively.

airspeed k^1 and a specific AoA k^2 , with the complete series covering the required range of each variable, say $[k_{min}^1, k_{max}^1]$ and $[k_{min}^2, k_{max}^2]$, via the discretizations $\{k_1^1, k_2^1, \dots, k_{M_1}^1\}$ and $\{k_1^2, k_2^2, \dots, k_{M_2}^2\}$. For the identification of a global VFP model the flight state vector \mathbf{k} containing the airspeed and AoA scalar components, is defined as:

$$\mathbf{k} = [k_i^1 \ k_j^2]^T \iff k_{i,j}, \quad i = 1, \dots, M_1, \quad j = 1, \dots, M_2 \quad (2)$$

with $k_{i,j}$ designating the flight state of the wing corresponding to the i -th airspeed and the j -th angle of attack. This procedure yields a pool of response signals (each of length N):

$$x_{\mathbf{k}}[t], y_{\mathbf{k}}[t] \quad \text{with} \quad t = 1, \dots, N, \quad k^1 \in \{k_1^1, \dots, k_{M_1}^1\},$$

$$\text{and} \quad k^2 \in \{k_1^2, \dots, k_{M_2}^2\}. \quad (3)$$

The VFP-AR model is of the following form (Refs. 7, 15):

$$y_{\mathbf{k}}[t] + \sum_{i=1}^n a_i(\mathbf{k}) \cdot y_{\mathbf{k}}[t-i] = e_{\mathbf{k}}[t] \quad (4)$$

$$e_{\mathbf{k}}[t] \sim \text{iid } \mathcal{N}(0, \sigma_e^2(\mathbf{k})) \quad \mathbf{k} \in \mathbb{R}^2 \quad (5)$$

$$a_i(\mathbf{k}) = \sum_{j=1}^p a_{i,j} \cdot G_j(\mathbf{k}) \quad (6)$$

$$E\{e_{k_{i,j}}[t] \cdot e_{k_{m,n}}[t-\tau]\} = \gamma_e[k_{i,j}, k_{m,n}] \cdot \delta[\tau] \quad (7)$$

with n designating the AR order, $y_{\mathbf{k}}[t]$ the sensor's response signal, and $e_{\mathbf{k}}[t]$ the model's residual (one-step-ahead prediction error) sequence, that is a white (serially uncorrelated) zero mean sequence with variance $\sigma_e^2(\mathbf{k})$. This may potentially be cross-correlated with its counterparts corresponding to different experiments (different \mathbf{k} 's). The symbol $E\{\cdot\}$ designates statistical expectation, $\delta[\tau]$ the Kronecker delta (equal to unity for $\tau = 0$ and equal to zero for $\tau \neq 0$), $\mathcal{N}(\cdot, \cdot)$ Gaussian distribution with the indicated mean and variance, and iid stands for identically independently distributed.

As (6) indicates, the AR parameters $a_i(\mathbf{k})$ are modeled as explicit functions of the flight vector \mathbf{k} (which contains the airspeed and AoA components) by belonging to p -dimensional functional subspace spanned by the mutually independent basis functions $G_1(\mathbf{k}), G_2(\mathbf{k}), \dots, G_p(\mathbf{k})$ (*functional basis*). The functional basis consists of polynomials of two variables (bivariate) obtained as tensor products from their corresponding univariate polynomials (Chebyshev, Legendre, Jacobi, and other families (Refs. 15, 16)). The constants $a_{i,j}$ designate the AR coefficients of projection.

The VFP-AR model of (4)–(7) is parameterized in terms of the parameter vector to be estimated from the measured signals:

$$\bar{\theta} = [a_{1,1} \ a_{1,2} \ \dots \ a_{i,j} \ \vdots \ \sigma_e^2(\mathbf{k})]^T \quad \forall \mathbf{k} \quad (8)$$

and may be written in linear regression form as:

$$y_{\mathbf{k}}[t] = [\varphi_{\mathbf{k}}^T[t] \otimes g^T(\mathbf{k})] \cdot \theta + e_{\mathbf{k}}[t] = \phi_{\mathbf{k}}^T[t] \cdot \theta + e_{\mathbf{k}}[t] \quad (9)$$

with:

$$\varphi_{\mathbf{k}}[t] := [-y_{\mathbf{k}}[t-1] \ \dots \ -y_{\mathbf{k}}[t-n]]_{[n \times 1]}^T \quad (10)$$

$$g(\mathbf{k}) := [G_1(\mathbf{k}) \ \dots \ G_p(\mathbf{k})]_{[p \times 1]}^T \quad (11)$$

$$\theta := [a_{1,1} \ a_{1,2} \ \dots \ a_{n,p}]_{[(np \times 1)]}^T \quad (12)$$

and T designating transposition and \otimes Kronecker product (Ref. 27, Chap. 7).

Pooling together the expressions (9) of the VFP-AR model corresponding to all flight vectors \mathbf{k} ($k_{1,1}, k_{1,2}, \dots, k_{M_1, M_2}$) considered in the experiments (cross-sectional pooling) yields:

$$\begin{bmatrix} y_{k_{1,1}}[t] \\ \vdots \\ y_{k_{M_1, M_2}}[t] \end{bmatrix} = \begin{bmatrix} \phi_{k_{1,1}}^T[t] \\ \vdots \\ \phi_{k_{M_1, M_2}}^T[t] \end{bmatrix} \cdot \theta + \begin{bmatrix} e_{k_{1,1}}[t] \\ \vdots \\ e_{k_{M_1, M_2}}[t] \end{bmatrix}. \quad (13)$$

Then, following substitution of the data for $t = 1, \dots, N$ the following expression is obtained:

$$y = \Phi \cdot \theta + e \quad (14)$$

with

$$y := \begin{bmatrix} y[1] \\ \vdots \\ y[N] \end{bmatrix}, \quad \Phi := \begin{bmatrix} \Phi[1] \\ \vdots \\ \Phi[N] \end{bmatrix}, \quad e := \begin{bmatrix} e[1] \\ \vdots \\ e[N] \end{bmatrix}. \quad (15)$$

Using the above linear regression framework, the projection coefficient vector θ can be efficiently estimated via minimization of the Weighted Least Squares (WLS) criterion:

$$J^{\text{WLS}} := \frac{1}{N} \sum_{t=1}^N e^T[t] \Gamma_{e[t]}^{-1} e[t] = \frac{1}{N} e^T \Gamma_e^{-1} e \quad (16)$$

which leads to the *Weighted Least Squares (WLS)* estimator:

$$\hat{\theta}^{\text{WLS}} = [\Phi^T \Gamma_e^{-1} \Phi]^{-1} [\Phi^T \Gamma_e^{-1} y]. \quad (17)$$

In these expressions $\Gamma_e = E\{ee^T\}$ ($\Gamma_e = \Gamma_{e[t]} \otimes I_N$, with I_N designating the $N \times N$ unity matrix) designates the residual covariance matrix, which is practically unavailable. Nevertheless, it may be consistently estimated by applying (in an initial step) Ordinary Least Squares (details in (Ref. 15)). Once $\hat{\theta}^{\text{WLS}}$ has been obtained, the final residual variance and residual covariance matrix estimates are obtained as:

$$\hat{\sigma}_e^2(\mathbf{k}, \hat{\theta}^{\text{WLS}}) = \frac{1}{N} \sum_{t=1}^N e_{\mathbf{k}}^2[t, \hat{\theta}^{\text{WLS}}],$$

$$\hat{\Gamma}_{e[t]} = \frac{1}{N} \sum_{t=1}^N e[t, \hat{\theta}^{\text{WLS}}] e^T[t, \hat{\theta}^{\text{WLS}}]. \quad (18)$$

The estimator $\hat{\theta}^{\text{WLS}}$ may, under mild conditions, be shown to be asymptotically Gaussian distributed with mean coinciding with the true parameter vector θ^o and covariance matrix P_θ

$$\sqrt{N}(\hat{\theta}_N - \theta^o) \sim \mathcal{N}(0, P_\theta) \quad (N \rightarrow \infty) \quad (1)$$

based on which interval estimates of the true parameter vector may be constructed (Ref. 15).

The problem of VFP-AR model structure selection (structure estimation) for a given basis function family (such as Chebyshev, Legendre, and so on), that is model order determination for the AR polynomial and determination of their corresponding functional subspaces, is referred to as the model identification problem. Usually, the AR model order is initially selected via customary model order selection techniques (BIC, RSS, frequency stabilization diagrams) (Ref. 24), whereas the functional subspace dimensionality is selected via a Genetic Algorithm (GA) procedure (Ref. 15). Initially, the maximum functional subspace dimensionality is selected, which defines the search space of the functional subspace estimation subproblem. The determination of the exact subspace dimensionality is achieved via the use of GAs based on minimization of the BIC with respect to the candidate basis functions. In the current study, the estimation of the functional subspace dimensionality was achieved via the use of the BIC criterion for increasing functional subspace dimensionality.

EXPERIMENTAL RESULTS

Non-parametric analysis

Figure 3 presents indicative wind tunnel signals obtained from piezoelectric sensor 2 under various AoA and freestream velocities of $U_\infty = 11$ m/s (top subplot) and $U_\infty = 15$ m/s (bottom subplot). Observe the stochastic (random) nature of these signals, which is due to the wind tunnel airflow actuation and the aeroelastic response of the wing. In addition, it is evident that for higher AoA and as the wing approaches stall, the signal amplitude (voltage) increases. In the case of $U_\infty = 11$ m/s (top subplot) in Figure 3, the maximum signal amplitude for AoA of 13 and 15 degrees seems to be similar as there is no evident further increase. For this freestream velocity and based on the airfoil properties and CFD analysis, stall occurs at an AoA of approximately 13 degrees. In the case of $U_\infty = 15$ m/s (bottom subplot) in Figure 3, stall occurs at approximately 15 degrees, and it may be readily observed that there is an obvious increase in the signal amplitude from 13 to 15 degrees AoA.

Non-parametric identification is based on 90,000 (90 s) sample-long response signals obtained from the embedded piezoelectric sensors (see Table 3). A 5096 sample-long Hamming data window (frequency resolution $\Delta f = 0.24$ Hz) with 90% overlap is used for the Welch-based spectral estimation (MATLAB² function *pwelch.m*).

²In this work Matlab version R2015b has been used.

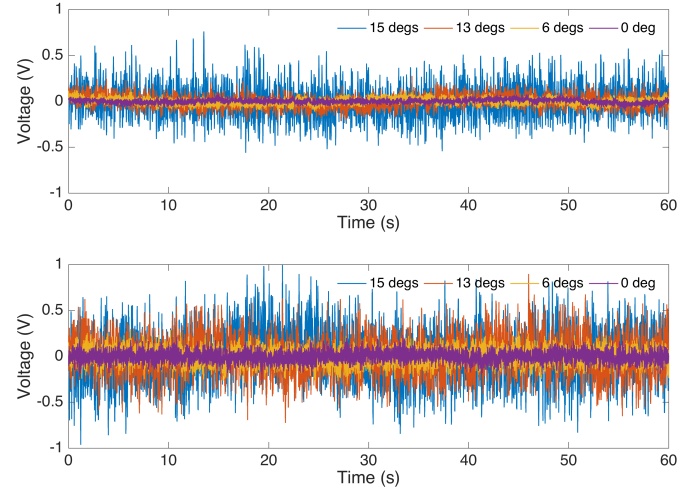


Fig. 3. Indicative signals obtained from piezoelectric sensor 1 under various angles of attack: (a) freestream velocity $U_\infty = 11$ m/s (top subplot) and (b) freestream velocity $U_\infty = 17$ m/s (bottom subplot).

Figure 4 presents indicative non-parametric power spectral density (PSD) Welch-based estimates obtained from piezoelectric sensor 1 for increasing airspeed and a constant AoA of 0 degrees within the [0.1 – 25] Hz frequency range (left subplot). Notice that as the airspeed increases, the PSD amplitude in the lower frequency range slightly increases as well. In this case, it is expected that as the airspeed increases for a constant AoA the wing will approach flutter which will be triggered by the coupling of aeroelastic modes. In this case the coupling occurs in the [0.5 – 15] Hz frequency range. By carefully observing Figure 4 it may be seen that the frequency at approximately 5 Hz increases with increasing airspeed and approaches the frequency at approximately 9 Hz, thus providing an indication of incipient flutter. This observation will be clarified by the global parametric modeling results.

Similarly, Figure 5 presents indicative non-parametric power spectral density (PSD) Welch-based estimates of the piezoelectric response signals obtained from sensor 1 for increasing AoA and freestream velocity $U_\infty = 15$ m/s (right subplot). Notice that as the AoA increases the PSD amplitude in the lower frequency range of [0.1 – 12] Hz significantly increases as well. More specifically, as the AoA approaches the critical stall range of [13 – 15] degrees, the low frequency vibrations become dominant and thus indicating the proximity to the stall of the wing. From this Figure it is evident that by monitoring the identified lower frequency bandwidths that are sensitive to increasing AoA it is possible to obtain a strong indication of stall. All the embedded piezoelectric sensors of the wing exhibit a similar performance, but for the sake of brevity the results are presently omitted.

Strain Distribution

Indicative results obtained from strain gauges 5 and 14 are presented in Figure 6 and Figure 7, respectively. The recorded

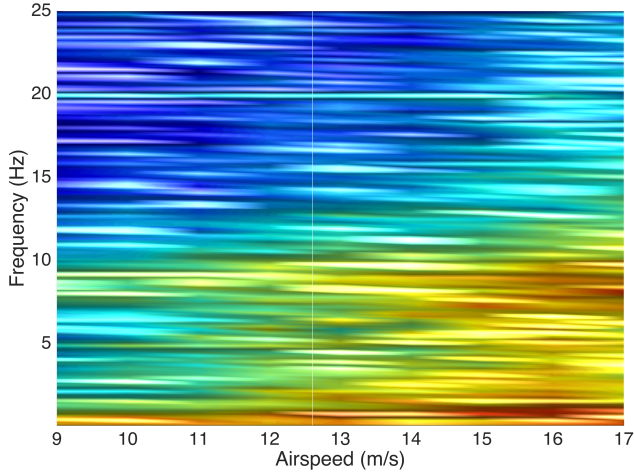


Fig. 4. Indicative non-parametric Welch-based power spectral density (PSD) estimates for piezoelectric sensor 1 versus varying airspeed with set AoA of 1 degree.

strain is plotted for increasing AoA and airspeed, hence the strain mapping for the specific location on the wing may be obtained for the considered experimental conditions. As the AoA and airspeed increase the applied strain also increases, with the maximum strain appearing, as expected, in the top right corner of the figures (for the maximum airspeed and AoA). The strain shown in these plots is estimated as the mean value of the acquired signal (9000 samples; 90 s). The maximum strain is observed for angles higher than 8 degrees and velocities higher than 16 m/s, resulting in a critical, with respect to strain, flying area of the wing that for the considered experimental conditions (or –in the more general concept–flight envelope) is located in the top right corner of the figures. Finally, the recorded strain is higher for gauge 5 than gauge 13. This is due to the fact that strain gauge 5 is closer to the root of the wing and thus it is expected that the quasi-static strain in that location should be higher than the strain closer to the wing tip.

Parametric analysis via global models

For the parametric identification, conventional autoregressive (AR) time-series models representing the wing's structural dynamics are obtained through standard identification procedures (Refs. 24, 25) based on the collected piezoelectric response signals (MATLAB function *arx.m*). The response signal bandwidth is selected as 0.1 – 30 Hz after the initial signals were low-pass filtered (Chebyshev Type II) and sub-sampled to a resulting sampling frequency $f_s = 60$ Hz (initial sampling frequency was 1000 Hz). Each signal resulted in a length of $N = 4,000$ samples (20 s) and was subsequently sample mean corrected.

The modeling strategy consists of the successive fitting of AR(n) models (with n designating the AR order) until a suitable model is selected. Model parameter estimation is achieved by minimizing a quadratic prediction error (PE) criterion leading to a least squares (LS) estimator (Ref. 24, p.

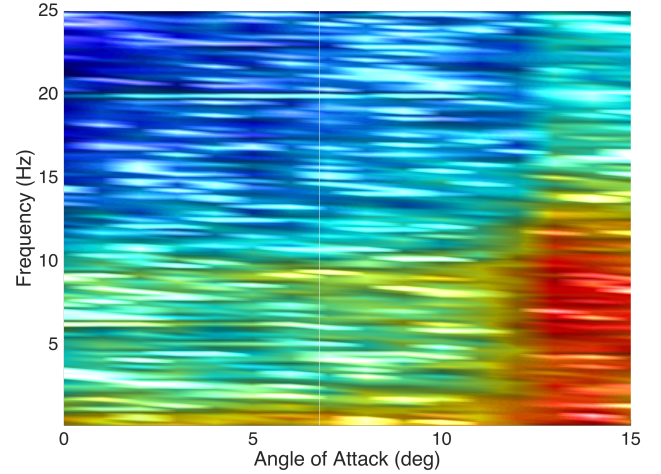


Fig. 5. Indicative non-parametric Welch-based power spectral density (PSD) estimates for piezoelectric sensor 1 versus varying AoA for set airspeed $U_\infty = 13$ m/s.

206). Model order selection, which is crucial for successful identification, may be based on a combination of tools, including the Bayesian information criterion (BIC), which is a statistical criterion that penalizes model complexity (order) as a counteraction to a decreasing quality criterion (Ref. 24, pp. 505–507), monitoring of the RSS/SSS (residual sum of squares/ signal sum of squares) criterion, monitoring of the residual autocorrelation function (MATLAB function *autocorr.m*) (Ref. 24, p. 512), and use of “stabilization diagrams” which depict the estimated modal parameters (usually frequencies) as a function of increasing model order (Refs. 24, 25).

For piezoelectric sensor 1, this leads to an AR(18) model for a collected data set corresponding to an airspeed of 11 m/s and an angle of attack of 3 degrees. This model is used as reference and for providing approximate orders for the identification of the global VFP-AR models of the next section. For the sake of brevity, in the following sections indicative results from sensor 1 only will be presented.

The global modeling of the composite wing is based on signals obtained from a total of $M_1 \times M_2 = 144$ experiments. Airspeeds up to 17 m/s and AoA up to 15 degrees were considered for the Vector-dependent Functionally Pooled (VFP) based modeling procedure. The airspeed and AoA increments are $\Delta k^1 = 1$ m/s and $\Delta k^2 = 1$ degree, respectively, covering the corresponding intervals of [9, 17] m/s and [0, 15] degrees.

Model order selection starts with the orders selected for the conventional AR models representing the wing structure for a constant indicative experimental condition. The final model orders being presently selected are based on the BIC criterion (Ref. 26) and model validation techniques, such as checking the whiteness (uncorrelatedness) and the normality of the model residuals (MATLAB functions *acf.m* and *normplot.m*, respectively) (Refs. 24, 26). The functional subspaces are selected via a similar BIC-based process. The functional subspace consists of 21 Chebyshev Type II bivariate polynomial

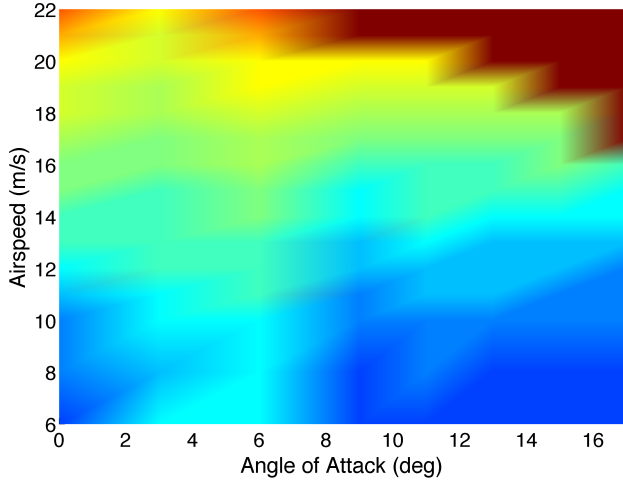


Fig. 6. Indicative strain distribution obtained from strain gauge 5 for the considered angles of attack and freestream velocities.

basis functions (Refs. 15–17).

The final identified global model is a VFP-AR(72)₂₄. The functional subspace consists of the first $p = 24$ shifted Chebyshev Type II 2-dimensional polynomials.

In this study, the identified VFP model is of significantly lower order than the corresponding results presented in (Ref. 7). This was to investigate a model that focuses on the lower frequencies (< 30 Hz) that are dominant in the structural response of the composite wing. This also reduces potential over-parametrization and significantly reduces the computational burden allowing for potential close to real-time model estimation.

Indicative VFP-model-based frequency response function (FRF) magnitude results obtained from the VFP-AR(18)₂₁ global model are depicted as functions of frequency and airspeed for set AoA 0 degrees in Figure 8. The frequency resolution is 0.01 Hz, while the airspeed resolution is 0.1 m/s. Observe how the wing mode at 4.5 Hz for airspeed 9 m/s gradually increases with the increasing airspeed until completely coupled with the mode at 9 Hz at approximately 16 m/s. This behavior of the aeroelastic modes of the wing, as identified by the VFP-AR model, corresponds to the generation of dynamic flutter. It may be readily observed that the results of Figure 8 are, as expected, extremely accurate when compared to the corresponding non-parametric Welch-based analysis of Figure 4. It is also worth mentioning that the non-parametric results of Figure 4 have been obtained using a significantly longer signal of 90 seconds, whereas the VFP-based parametric results are based on 20-second-long signals.

The VFP-model-based FRF magnitude curves obtained via the VFP-AR(18)₂₁ global model are depicted as functions of frequency and AoA in the right plot in Figure 9. The frequency resolution is 0.01 Hz, while the AoA resolution is 0.1 degrees. The airspeed of 15 m/s is very close to the occurrence of flutter and the wing exhibits two distinct aeroelastic modes within the [5 – 10] Hz range. However, observe that for

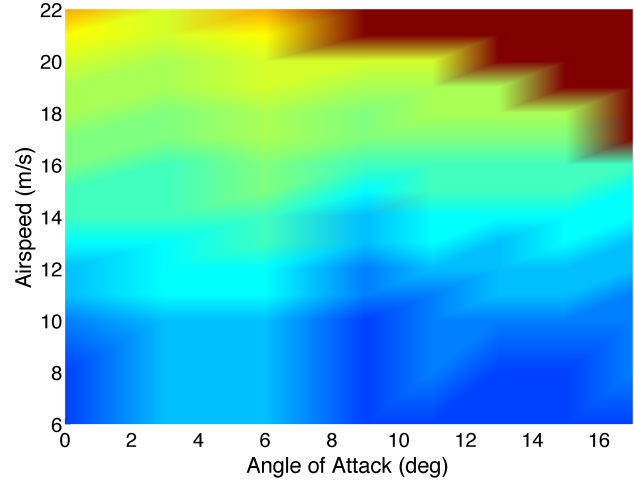


Fig. 7. Indicative strain distribution obtained from strain gauge 13 for the considered angles of attack and freestream velocities.

an AoA of 0 degrees, the modes are very close and almost coincide, which is in agreement with Figure 8 that presents the model-based FRF for set AoA of 0 degrees versus increasing airspeed. By observing the frequency evolution versus the AoA it may be assessed that the amplitude of the VFP-based FRF magnitude increases for lower frequencies (< 15 Hz) with increasing AoA as the wing approaches stall. More specifically, the FRF magnitude exhibits a sharp increase for AoA higher than 13 degrees in which stall occurs.

By comparing the VFP-based parametric FRF magnitudes with the corresponding non-parametric Welch-based spectral estimates of Figure 5 it may be concluded that high accuracy is achieved by the global modeling approach which also employs a significantly shorter signal length (see Table 3).

ACTIVE SENSING SHM

SHM technologies, oftentimes in combination with appropriate NDE and/or HUMS, along with sophisticated data management systems and life-prediction models, address the formulation of the required steps for the transition to condition-based maintenance (CBM) and complete structural awareness for safety assurance. In this section, the application of an acousto-ultrasound active sensing SHM approach is presented for the intelligent composite wing. Apart from the passive sensing of the ambient vibration (aeroelastic) response of the wing via the embedded piezoelectric sensor network, the same network can be used in an active sensing mode to perform pulse-echo or pitch-catch guided-wave-based diagnostic SHM. Piezoelectric sensors-actuators can be used both as transmitters and receivers for monitoring local defects by injecting controlled diagnostic signals into structures and can potentially interrogate large structural areas. In principle, an active system allows damage to be interrogated by injecting controlled diagnostic signals (i.e. guided Lamb waves) into the structure. With the known inputs, the changes in local

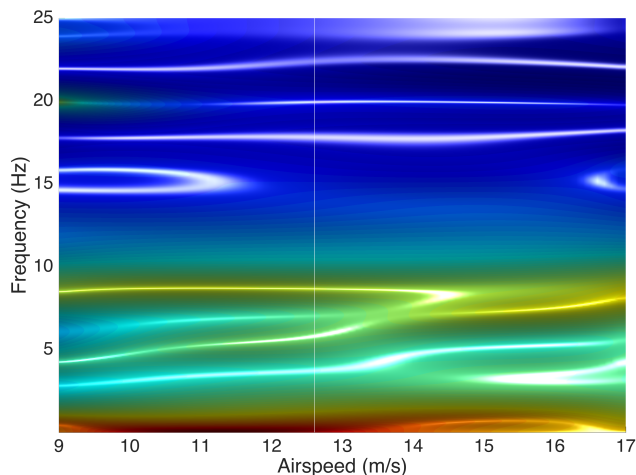


Fig. 8. Indicative parametric FRF magnitude results based on the VFP-AR(18)₂₁ global model as a function of frequency and airspeed for set AoA of 0 degrees.

sensor measurements are associated with the introduction of damage in the structure.

The use of distributed piezoelectric sensors embedded inside the wing allows for the development of in-situ, on-demand, diagnostic approaches that tackle damage detection, localization, and quantification; the present study focuses on the detection and localization tasks. The distributed network is expected to increase the damage localization and quantification accuracy and robustness, that is the topic of on-going work by the authors and co-workers (Refs. 28,29). Increasing the damage quantification robustness of active sensing ultrasound approaches for hotspot monitoring can be achieved via the use of multiple sensors, and thus wave propagation paths (Ref. 29). As the number of sensors and propagation paths increases, the uncertainty in the damage index (as defined in (Ref. 28)) will decrease leading to robust damage quantification. Theoretically, it is assumed that the damage index value will converge to its “real” value as the number of sensors/paths increases, as the addition of new paths will not contribute to any useful information (Ref. 29).

Figure 10 presents indicative structural health monitoring results based on a series of experiments performed on the composite wing under controlled laboratory environment and during the wind tunnel experiments. Ultrasound guided 5-peak tone-burst waves were generated from the embedded piezoelectric transducers acting as actuators for a number of center frequencies, spanning the range of 100 – 700 kHz. The ultrasound waves were recorded by piezoelectric transducers acting as sensors and mounted on three sensing topologies on the wing. These topologies were defined in terms of a hotspot monitoring scenario, such as that specific locations on the wing are considered to be prone to the appearance of damage. In this case, the three topologies cover the complete area of the wing and employ 19 piezoelectric sensors embedded in the composite layup. The location of the sensors and the corresponding topologies are shown in Figure 10.

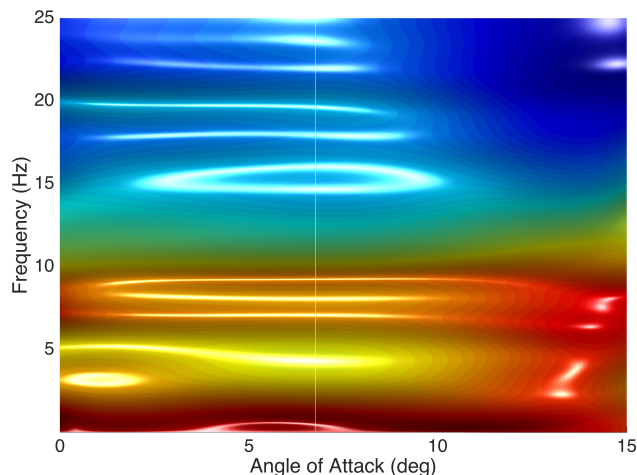


Fig. 9. Indicative parametric FRF magnitude results based on the VFP-AR(18)₂₁ global model as a function of frequency and AoA for set airspeed of 15 m/s.

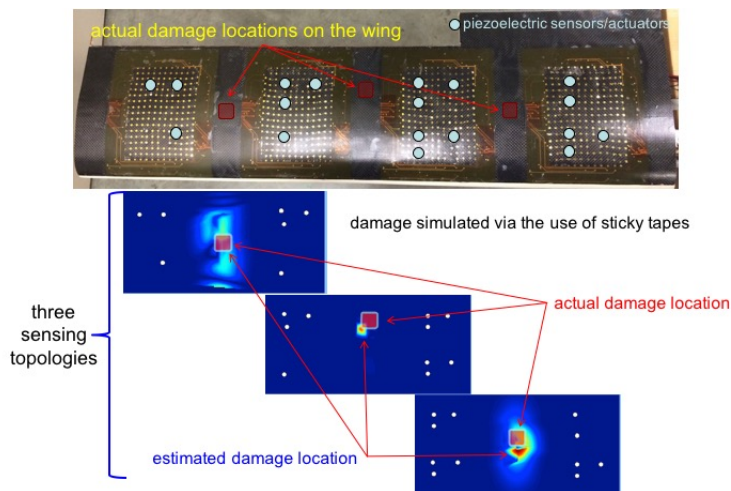


Fig. 10. Indicative structural health monitoring results based on the active-sensing acousto-ultrasound approach (Ref. 28) for a center frequency of 250 kHz.

Simulated damage was introduced in various locations on the wing by attaching lightweight sticky tapes. The active sensing approach employed in this study is based on the damage index (DI) defined in the recent work of (Ref. 28). The indicative results of Figure 10 for a center wave frequency of 250 kHz indicate that the method is able to detect and localize the existence of artificial damage. The actual damage location is indicated via the red rectangular areas, while the estimated damage location is indicated by the diagnostic image (for more details the interested reader is referred to (Ref. 5)).

In addition, the method was applied during the wind tunnel experiments and is the topic of on-going work to be presented in a subsequent article.

CONCLUSIONS

The objective of this work was to outline the main design, fabrication, and data modeling and analysis challenges of a self-sensing self-diagnostic intelligent composite UAV wing with state sensing and awareness capabilities. The embedded bio-inspired stretchable sensor networks consisting of piezoelectric, strain gauges, and RTDs enabled the data-driven identification of the coupled structural and aerodynamic properties under varying flight states and uncertainty. Piezoelectric sensors were used in two modes: (i) passive mode to sense the ambient vibration of the wing in order to identify the coupled airflow-structural dynamics and related them to critical aerodynamic/aeroelastic phenomena such as stall and flutter; (ii) active mode, as both actuators and sensors to implement an active sensing acousto-ultrasound pitch-catch SHM approach.

Special emphasis was given to the wind tunnel experimental assessment under various flight states defined by multiple airspeeds and angles of attack. A novel modeling approach based on the recently introduced Vector-dependent Functionally Pooled (VFP) model structure was employed for the stochastic data-driven modeling of the global aeroelastic vibration response of the wing. In addition, the strain distribution was established under the considered flight states and critical areas—as defined by increased strain signatures—of the flight envelope were identified. The obtained results demonstrated the successful integration of the micro-fabricated stretchable sensor networks with the composite materials of the wing, as well as the effectiveness of the stochastic VFP-based “global” modeling and active sensing SHM approaches, proving their integration potential for the next generation of self-sensing self-diagnostic aerial vehicles and aerospace structures.

Author contact: Fotis Kopsaftopoulos kopsaf@rpi.edu and Fu-Kuo Chang fkchang@stanford.edu

ACKNOWLEDGMENTS

This experiments and preliminary analysis for this work were supported by the U.S. Air Force Office of Scientific Research (AFOSR) program “Avian-Inspired Multifunctional Morphing Vehicles” under grant FA9550-16-1-0087 with Program Manager Byung-Lip (“Les”) Lee. The author would like to thank Mr. Raphael Nardari and Dr. Yu-Hung Li at Stanford University for their contribution in the design and fabrication of the composite wing and sensor networks.

REFERENCES

¹Salowitz, N., Guo, Z., Roy, S., Nardari, R., Li, Y.-H., Kim, S.-J., Kopsaftopoulos, F., and Chang, F.-K., “Recent advancements and vision toward stretchable bio-inspired networks for intelligent structures,” *Structural Health Monitoring*, Vol. 13, (6), 2014, pp. 609–620.

²Kopsaftopoulos, F., Nardari, R., Li, Y.-H., and Chang, F.-K., “Experimental identification of structural dynamics

and aeroelastic properties of a self-sensing smart composite wing,” *Structural Health Monitoring 2015: System Reliability for Verification and Implementation – Proceedings of the 10th International Workshop on Structural Health Monitoring (IWSHM 2015)*, edited by F.-K. Chang and F. Kopsaftopoulos, September 2015.

³Suryakumar, V. S., Babbar, Y., Strganac, T. W., and Mangalam, A. S., “Control of a Nonlinear Wing Section using Fly-by-Feel Sensing,” *AIAA Atmospheric Flight Mechanics Conference*, 2015.

⁴Kopsaftopoulos, F., Nardari, R., Li, Y.-H., Wang, P., and Chang, F.-K., “Stochastic global identification of a bio-inspired self-sensing composite UAV wing via wind tunnel experiments,” *Proceedings of the SPIE 9805, Health Monitoring of Structural and Biological Systems 2016*, 98051V, April 2016.

⁵Ihn, J. and Chang, F.-K., “Pitch-catch active sensing methods in structural health monitoring for aircraft structures,” *Structural Health Monitoring*, Vol. 7, (1), 2008, pp. 5–19.

⁶Zhuang, Y., Kopsaftopoulos, F., and Chang, F.-K., “Bond-line integrity monitoring of adhesively bonded structures via an electromechanical impedance based approach,” *Structural Health Monitoring 2015: System Reliability for Verification and Implementation – Proceedings of the 10th International Workshop on Structural Health Monitoring (IWSHM 2015)*, edited by F.-K. Chang and F. Kopsaftopoulos, Vol. 2, 2015.

⁷Kopsaftopoulos, F., Nardari, R., Li, Y.-H., and Chang, F.-K., “A stochastic global identification framework for aerospace structures operating under varying flight states,” *Mechanical Systems and Signal Processing*, Vol. 98, 2018, pp. 425–447.
doi: 10.1016/j.ymsp.2017.05.001

⁸Kopsaftopoulos, F., Nardari, R., Li, Y.-H., and Chang, F.-K., “Data-driven state awareness for fly-by-feel aerial vehicles: Experimental assessment of a non-parametric probabilistic stall detection approach,” *Structural Health Monitoring 2017: Real-Time Material State Awareness and Data-Driven Safety Assurance – Proceedings of the 11th International Workshop on Structural Health Monitoring (IWSHM 2017)*, edited by F.-K. Chang and F. Kopsaftopoulos, September 2017.

⁹Lanzara, G., Salowitz, N., Guo, Z., and Chang, F.-K., “A spider-web-like highly expandable sensor network for multifunctional materials,” *Advanced Materials*, Vol. 22, (41), 2010, pp. 4643–4648.

¹⁰Dowell, E., Edwards, J., and Strganac, T., “Nonlinear aeroelasticity,” *Journal of aircraft*, Vol. 40, (5), 2003, pp. 857–874.

¹¹Livne, E., “Future of airplane aeroelasticity,” *Journal of Aircraft*, Vol. 40, (6), 2003, pp. 1066–1092.

- ¹²Georgiou, G., Manan, A., and Cooper, J., “Modeling composite wing aeroelastic behavior with uncertain damage severity and material properties,” *Mechanical Systems and Signal Processing*, Vol. 32, 2012, pp. 32–43.
- ¹³Jones, J. and Cesnik, C., “Nonlinear Aeroelastic Analysis of the X-56A Multi-Utility Aeroelastic Demonstrator,” Proceedings of 5th Dynamics Specialists Conference, January 2016.
- ¹⁴Kitson, R. C. and Cesnik, C. E., “Aeroelastic Modeling and Simulation of High-Speed Flexible Vehicles,” 15th Dynamics Specialists Conference, 2016.
- ¹⁵Kopsaftopoulos, F. P. and Fassois, S. D., “Vector-dependent Functionally Pooled ARX models for the identification of systems under multiple operating conditions,” Proceedings of the 16th IFAC Symposium on System Identification, (SYSID), July 2012.
- ¹⁶Kopsaftopoulos, F. P., *Advanced Functional and Sequential Statistical Time Series Methods for Damage Diagnosis in Mechanical Structures*, Ph.D. thesis, Department of Mechanical Engineering & Aeronautics, University of Patras, Patras, Greece, January 2012.
- ¹⁷Kopsaftopoulos, F. P. and Fassois, S. D., “A Functional Model Based Statistical Time Series Method for Vibration Based Damage Detection, Localization, and Magnitude Estimation,” *Mechanical Systems and Signal Processing*, Vol. 39, 2013, pp. 143–161.
doi: 10.1016/j.ymssp.2012.08.023
- ¹⁸Salowitz, N., Guo, Z., Li, Y.-H., Kim, K., Lanzara, G., and Chang, F.-K., “Bio-inspired stretchable network-based intelligent composites,” *Journal of Composite Materials*, Vol. 47, (1), 2013, pp. 97–106.
- ¹⁹Guo, Z., Kim, K., Lanzara, G., Salowitz, N., Peumans, P., and F.-K.Chang, “Bio-inspired smart skin based on expandable network,” Proceedings of the 8th International Workshop on Structural Health Monitoring 2011 - Condition Based Maintenance and Intelligent Structures, edited by F.-K. Chang, September 2011.
- ²⁰Salowitz, N., Guo, Z., Kim, S.-J., Li, Y.-H., Lanzara, G., and Chang, F.-K., “Screen-printed piezoceramic actuators/sensors microfabricated on organic films and stretchable networks,” Proceedings of the 9th International Workshop on Structural Health Monitoring 2013, edited by F.-K. Chang, September 2013.
- ²¹Guo, Z., *Robust Design And Fabrication Of Highly Stretchable Sensor Networks For The Creation Of Intelligent Materials*, Ph.D. thesis, Department of Aeronautics and Astronautics, Stanford University, 2014.
- ²²Salowitz, N., Guo, Z., Roy, S., Nardari, R., Li, Y.-H., Kim, S., Kopsaftopoulos, F., and Chang, F.-K., “A vision on stretchable bio-inspired networks for intelligent structures,” Proceedings of the 9th International Workshop on Structural Health Monitoring (IWSHM 2013), edited by F.-K. Chang, September 2013.
- ²³Sakellariou, J. S. and Fassois, S. D., “Functionally Pooled models for the global identification of stochastic systems under different pseudo-static operating conditions,” *Mechanical Systems and Signal Processing*, Vol. 72-73, 2016, pp. 785807. doi: 10.1016/j.ymssp.2015.10.018
- ²⁴Ljung, L., *System Identification: Theory for the User*, Prentice–Hall, second edition, 1999.
- ²⁵Söderström, T. and Stoica, P., *System Identification*, Prentice–Hall, 1989.
- ²⁶Fassois, S. D., “Parametric identification of vibrating structures,” *Encyclopedia of Vibration*, edited by S. Braun, D. Ewins, and S. Rao, Academic Press, 2001, pp. 673–685.
- ²⁷Bernstein, D., *Matrix Mathematics*, Princeton University Press, 2005.
- ²⁸Janapati, V., Kopsaftopoulos, F., Li, F., Lee, S., and Chang, F.-K., “Damage detection sensitivity characterization of acousto-ultrasound-based structural health monitoring techniques,” *Structural Health Monitoring*, Vol. 15, (2), 2016, pp. 143–161.
- ²⁹Yadav, S., Chung, H., Kopsaftopoulos, F., and Chang, F.-K., “Damage quantification of active-sensing acousto-ultrasound-based SHM via a multi-path unit-cell approach,” *Structural Health Monitoring 2017: Real-Time Material State Awareness and Data-Driven Safety Assurance – Proceedings of the 11th International Workshop on Structural Health Monitoring (IWSHM 2017)*, edited by F.-K. Chang and F. Kopsaftopoulos, September 2017.